Electronic Seismologist

MISARA: Matlab Interface for Seismo-Acoustic aRray Analysis

Vittorio Minio[1], Luciano Zuccarello[*2,3], Silvio De Angelis[2,3], Giuseppe Di Grazia[4], and Gilberto Saccorotti[2]

Abstract

Volcanic activity produces a broad spectrum of seismic and acoustic signals whose characteristics provide important clues on the underlying magmatic processes. Networks and arrays of seismic and acoustic sensors are the backbone of most modern volcano monitoring programs. Investigation of the signals gathered by these instruments requires efficient workflows and specialist software. The high sampling rates, typically 50 Hz or greater, at which seismic and acoustic waveforms are recorded by multistation networks and dense arrays leads to the rapid accumulation of large volumes of data, making the implementation of efficient data analysis workflows for volcano surveillance a challenging task. Here, we present an open-source MATLAB graphical user interface, MISARA (Matlab Interface for Seismo-Acoustic aRray Analysis), designed to provide a user-friendly workflow for the analysis of seismoacoustic data in volcanic environments. MISARA includes efficient algorithm implementations of well-established techniques for seismic and acoustic data analysis. It is designed to support visualization, characterization, detection, and location of volcano seismoacoustic signals. Its intuitive, modular, structure facilitates rapid, semiautomated, inspection of data and results, thus reducing user effort. MISARA was tested using seismoacoustic data recorded at Etna Volcano (Italy) in 2010, 2011, and 2019, and is intended for use in education and research, and to support routine data analysis at volcano observatories.

Cite this article as Minio, V., L. Zuccarello, S. De Angelis, G. Di Grazia, and G. Saccorotti (2023). MISARA: Matlab Interface for Seismo-Acoustic aRray Analysis, *Seismol. Res. Lett.* **94**, 1689–1702, doi: 10.1785/0220220267.

Introduction

Volcano seismology deals with a large variety of seismic and acoustic signals (e.g., McNutt *et al.*, 2015). The analysis of these waveforms plays a key role in the surveillance of volcanoes and provides important insights on magmatic and hydrothermal processes in the plumbing system (e.g., Sparks *et al.*, 2012; Chouet and Matoza, 2013; McNutt *et al.*, 2015). The investigation of the wavefield properties of these signals and their source location is crucial for effective volcano monitoring. The application of traditional travel-time inversion methods to data from sparse networks, in particular to signals with emergent onsets such as long-period (LP) or very long period (VLP) earthquakes and volcanic tremor, is challenging. Owing to the nature of these signals, alternative localization methods have been used in the recent years, including amplitude-based techniques (Di Grazia *et al.*, 2006; Carbone *et al.*, 2008; Cannata *et al.*, 2013; Morioka *et al.*, 2017) and array methods (e.g., Rost and Thomas, 2002).

Seismic and acoustic arrays consist of multiple sensors arranged in clusters on a spatial scale significantly shorter than the wavelength of interest. In array analysis, the waveforms recorded by each sensor are processed together based on the common waveform model of the signal (Aki and Richards, 1980). Depending on the wave propagation model (i.e., plane vs. spherical wavefronts), a source location can be inferred directly or from backpropagation of the wave vectors determined from the coherent wavefield propagation across the array (Havskov and Alguacil, 2016). Several studies have employed array techniques to investigate the evolution of seismic and acoustic sources during periods of volcanic unrest (Saccorotti *et al.*, 2004; Di Lieto *et al.*, 2007; Inza *et al.*, 2014; Eibl *et al.*, 2017; De Angelis *et al.*, 2020, 2021; Zuccarello *et al.*, 2022), although their use as a monitoring tool remains limited (e.g., Coombs *et al.*, 2018).

1. Dipartimento di Scienze Biologiche, Geologiche ed Ambientali - Sezione di Scienze della Terra, Università degli Studi di Catania, Catania, Italy, https://orcid.org/0000-0003-4864-6049 (VM); 2. Istituto Nazionale di Geofisica e Vulcanologia, Sezione di Pisa, Pisa, Italy, https://orcid.org/0000-0003-0094-9577 (LZ); https://orcid.org/0000-0003-2636-3056 (SDA); https://orcid.org/0000-0003-2915-1446 (GS); 3. School of Environmental Sciences, University of Liverpool, Liverpool, United Kingdom; 4. Istituto Nazionale di Geofisica e Vulcanologia, Sezione di Catania-Osservatorio Etneo, Catania, Italy, https://orcid.org/0000-0002-8153-9280 (GDG)

*Corresponding author: luciano.zuccarello@ingv.it

Over the past decade, the amount of seismic and acoustic monitoring data gathered on active volcanoes has grown tremendously, making their analysis a challenging task. At the same time, a plethora of software packages and algorithms for signal processing were developed in different programming environments, including the Python and MATLAB platforms. The majority of these packages provide a broad range of command-line functionalities for the management and handling of waveform data and related metadata; examples include ObsPy (Beyreuther *et al.*, 2010), SEIZMO (Euler, 2014), and GISMO (Thompson and Reyes., 2018). Other toolboxes were designed with a narrower focus on signal processing, including spectral analyses, and event detection and classification (e.g., Lesage, 2009; Messina and Langer, 2011; Bueno *et al.*, 2020; Cortés *et al.*, 2021). Finally, other packages were developed to specifically perform seismic array analyses (e.g., Pignatelli *et al.*, 2008; Smith and Bean, 2020).

Here, we present MISARA (Matlab Interface for the Seismo-Acoustic aRary Analysis)—a MATLAB graphical user interface (GUI) that supports visualization, detection, and localization of volcano seismic and acoustic signals, with a focus on array techniques. In this article, we will introduce the main features and functionalities of MISARA. We will demonstrate its use and showcase the capabilities of the software in analyzing volcano seismic and acoustic waveforms, and discuss its suitability for both research and monitoring purposes.

Overview of MISARA

MISARA is an open-source MATLAB interface developed to support users with the application of array techniques to seismic and acoustic signals. It is characterized by an intuitive and modular structure. MISARA is organized into different classes and modules, and its functionalities are accessed through several GUI windows (Fig. 1).

Home window

The Home window (Fig. 2) is the control panel of MISARA, which allows to manage all aspects of data processing, including the configuration of the data source, input–output options, and the parametrization of all analyses that will be performed on the selected data. The Home panel includes four dynamic menus to independently manage, save, and import settings from the last analysis performed or to load a suite of default analysis parameters. It allows access to all other modules of MISARA for seismic and acoustic data processing.

Data preparation window

MISARA includes a module dedicated to the creation of appropriate data structures, that is, the create dataset module (Fig. 3), which is accessed via the data preparation window. MISARA works with seismic and acoustic waveforms archived as MATLAB structure arrays in a dedicated folder–file structure. These files contain the raw data and some relevant metadata (e.g., station name, sampling rate, timing of records, etc.). MISARA modules require two additional files, which contain MATLAB structures providing the station coordinates and information on the instrument response, respectively.

The software can operate in two modes, depending on whether the data source is an offline archive or a web-based data server. In the offline mode, the user can read and convert common file formats into MISARA structures; these formats include the Seismic Analysis Code (SAC; Goldstein *et al.*, 2003; Goldstein and Snoke, 2005), Standard for the Exchange of Earthquake Data (SEED–miniSEED), and DSS Cube–Data Cube3 file format (see Data and Resources). In the other mode, the user can access data stored at the Incorporated Research Institutions for Seismology Data Management Center via International Federation of Digital Seismograph Networks services (see Data and Resources) to retrieve waveforms and station–channel metadata. The offline mode allows to recover information from XML files (eXtensible Markup Language). However, when XML files are not available, it is still possible to manually input station coordinates and instrument response parameters.

MISARA modules

All modules of MISARA share a similar design and workflow. All analysis and visualization parameters can be customized (Fig. 4). The data preprocessing modules (Fig. 1) are designed to perform data quality checks and to deconvolve the instrument response from the raw seismograms similarly to other MATLAB codes (e.g., Haney *et al.*, 2012; Thompson and Reyes, 2018). For seismic and acoustic array analyses, the data preprocessing modules also allow the user to evaluate the array response function using the Beam Pattern algorithm of Capon (1969). The signal features modules (Fig. 1) adopt well-established routines and algorithms for seismic and acoustic signal processing, such as spectrograms (Schlindwein *et al.*, 1995) and coherograms (Welch, 1967), root mean square (rms; Kenney and Keeping, 1962), polarization analysis (Jurkevics, 1988), short-term average/long-term average (STA/LTA; Allen, 1978), and the Sub-band Automatic LP Events Detection (SALPED; Garcia *et al.*, 2017).

The array modules (Fig. 1) implement several array processing algorithms for source localization of seismic and acoustic signals. This tool includes the zero lag cross-correlation (ZLC) analysis (Frankel *et al.*, 1991), MUltiple SIgnal Classification (Schmidt, 1986) algorithm, semblance, and radial semblance methods (Almendros *et al.*, 2002). For the evaluation of uncertainties in the estimate of the source position, we have implemented the JackKnife method (Efron, 1982). Additional details on all MISARA utilities are available in the help section of the software and the detailed user manual included in the public release of the software (see Data and Resources).

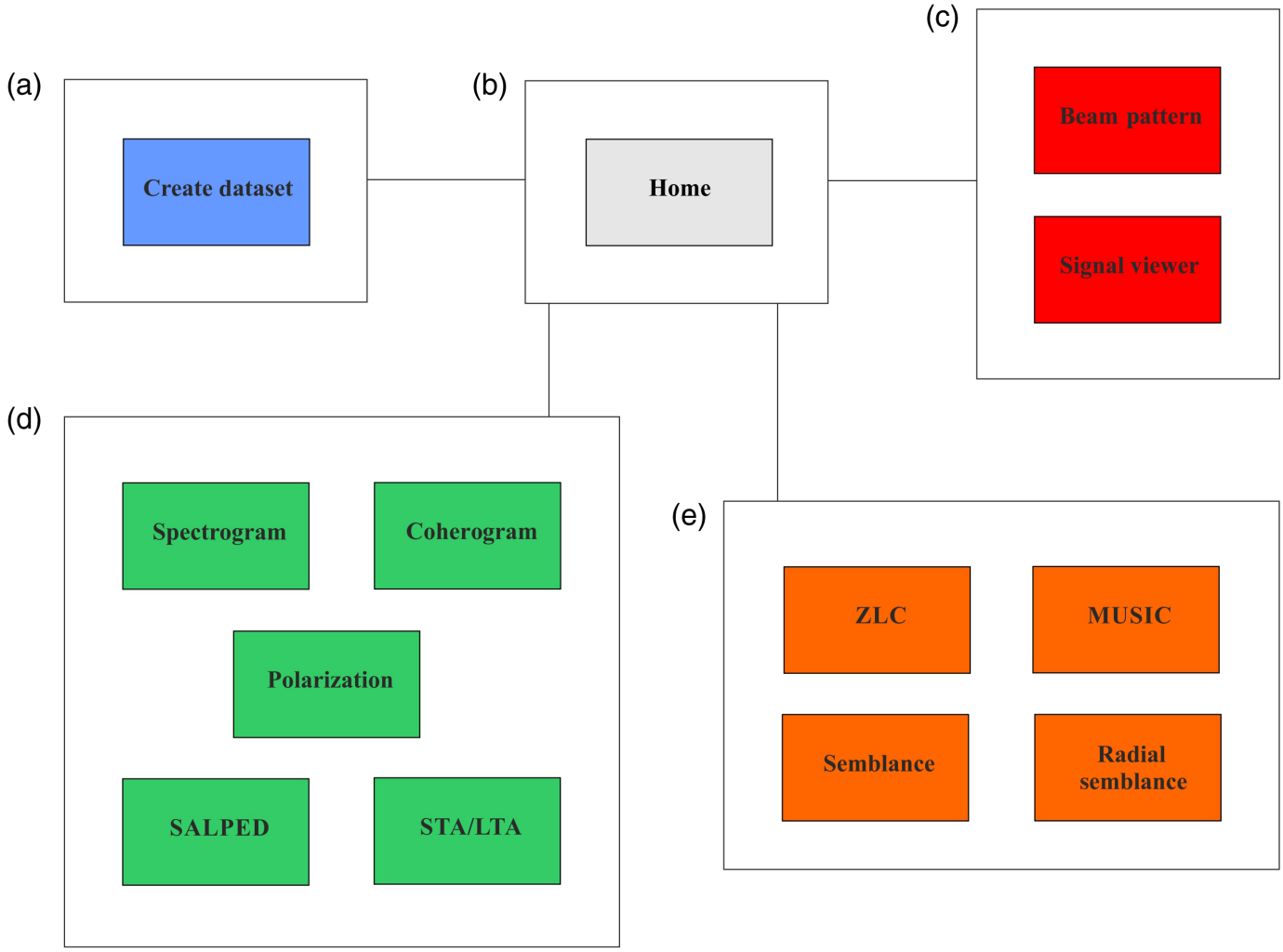

Figure 1. Overview of Matlab Interface for Seismo-Acoustic aRray Analysis (MISARA). (a) Data preparation window for data preparation and formatting. (b) Home window, the main panel for management of all functionalities of MISARA. (c) Data preprocessing modules for data quality control. (d) Signal features modules provide access to data processing, including array, spectral, polarization, location, and detection analysis. (e) Array analysis modules for source location methods based on multichannel techniques. The color version of this figure is available only in the electronic edition.

Examples

Here, we demonstrate the use and performances of MISARA through application to three cases studies. First, we perform analysis of volcanic tremor recorded by a seismic array deployed at Mt. Etna (Italy) in 2011 during intense lava fountain activity from its New Southeast Crater (NSEC). Second, we demonstrate the location of LP and VLP earthquakes recorded by the Mt. Etna permanent seismic network in 2010, which accompanied explosive activity at the Bocca Nuova (BN) crater. Finally, we show the analysis the infrasound data recorded by an infrasound array deployed at Mt. Etna in 2019, when the NSEC crater produced intense Strombolian activity. Detailed instructions on how to use of MISARA to reproduce the analyses shown here are available consulting the user manual and the video tutorials provided with the latest software release.

Case study 1: Mt. Etna, 2011 seismic array

MISARA was tested using offline data from a small-aperture seismic array deployed at Mt. Etna, Italy. The software configuration and its performances are summarized in Table A1. For this test, we used the beam pattern module to display the location of the array (Fig. 5a), its geometry (Fig. 5b), and to evaluate its response function at a selected target frequency (Fig. 5c). The array consisted of five single-component seismometers with an aperture of approximately 200 m, deployed at about 1 km from NSEC. Figure 5c, suggests that the configuration of the array allows reliable array analyses in the frequency band 1–3.0 Hz, which coincides with the dominant energy of volcanic tremor at Etna Volcano (e.g., Cannata *et al.*, 2010). We note that the array has poor resolution at low frequencies (0.5 Hz) caused by a signal wavelength larger than its aperture. On the other hand, the sensitivity and

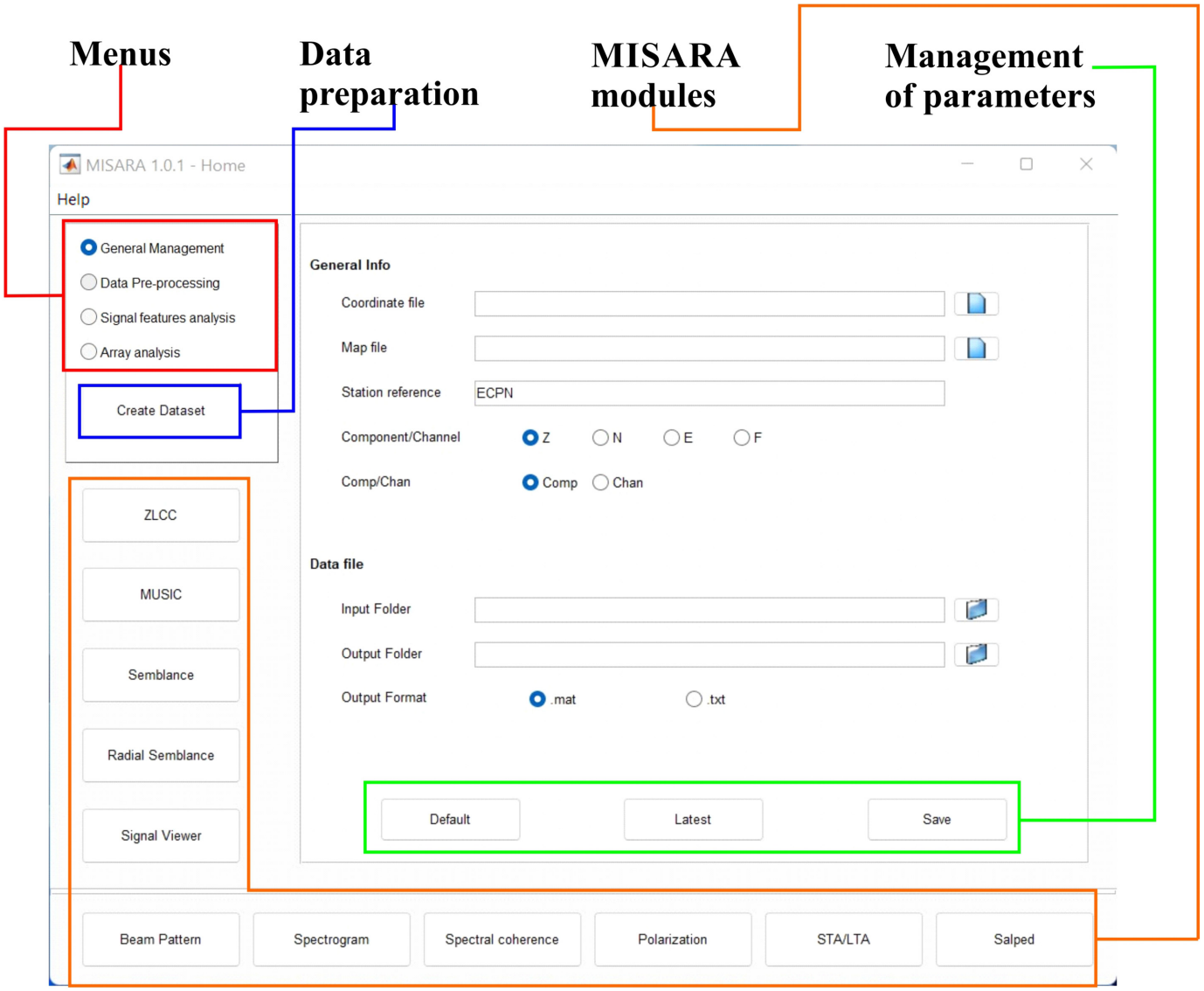

Figure 2. Screenshot of the Home window, showing a selection of configurable input parameters, and access to modules for data formatting and analysis. The color version of this figure is available only in the electronic edition.

resolution of the array is appropriate to investigate signals at frequencies up to 3 Hz. Aliasing becomes prevalent above 3 Hz. In the example shown in this article, array processing was performed using vertical-component seismograms. The use of horizontal components for seismic beamforming is also possible, although the user should consider limitations discussed in the more recent literature on the subject (e.g., Löer *et al.*, 2018; Wathelet *et al.*, 2018).

The spectral features and source location of volcanic tremor were investigated using the spectrogram and ZLC modules, respectively. An example of analysis of volcanic tremor, recorded during a lava fountain episode on 30 July 2011 at NSEC, is shown in Figure 6. The results include time series of back azimuth, ray parameter, tremor amplitude (rms), and spectrogram linked to changes in eruptive activity. Significant variations in amplitude, frequency content, and source location of tremor preceded and accompanied the onset of paroxysmal activity, which corresponded to shifts in the style and location of activity across different craters in the summit area of Mt. Etna (e.g., Patanè *et al.*, 2013; Moschella *et al.*, 2018). Figure 6a shows back azimuths dominantly between −15° and 5° N until about 7:00 a.m. (UTC) on 30 July, pointing toward the north-northeast sector of Mt. Etna (Fig. 6f); between 7:00 and 8:00 a.m. (UTC), which is 12 hr before the onset of lava fountain activity, the back azimuth gradually migrated to 30°–50° N (Fig. 6a), corresponding to the NSEC direction (Fig. 6f).

Case study 2: Mt. Etna, 2010 permanent seismic network

We also show the results of using MISARA with data recorded by the permanent seismic network operated by the Istituto

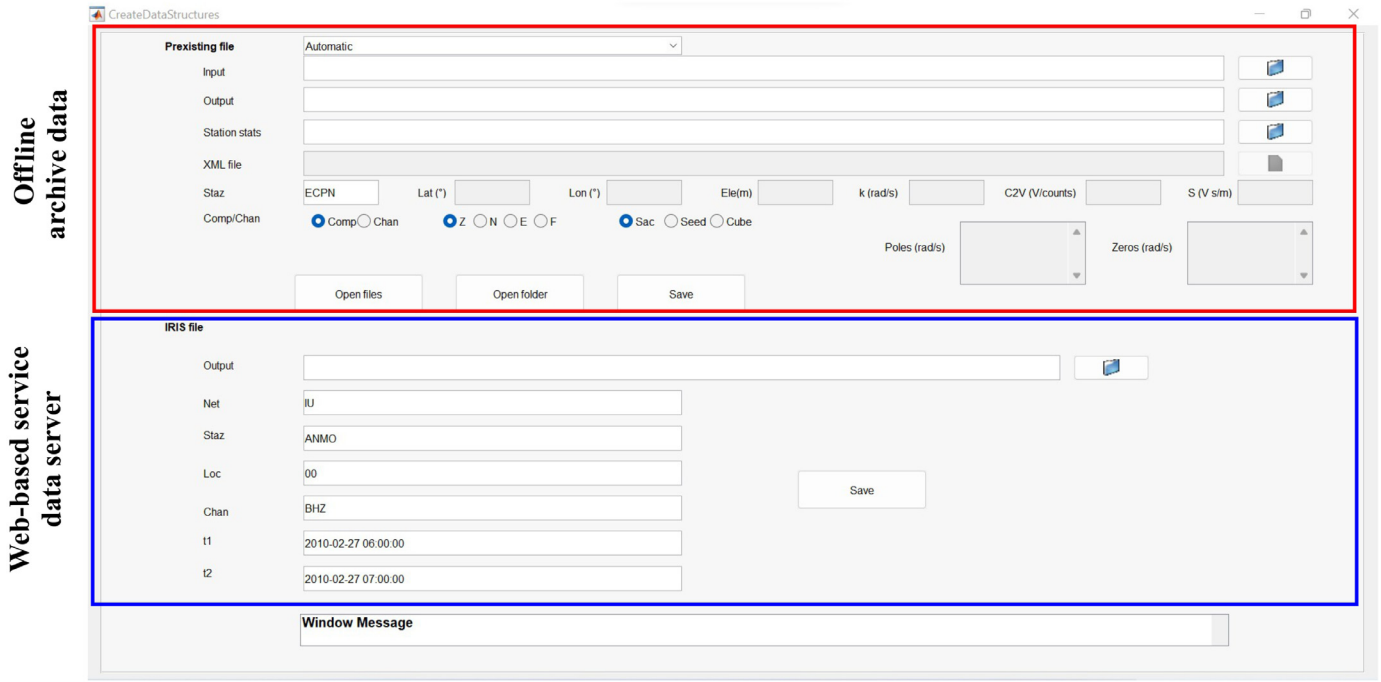

Figure 3. Screenshot of the create dataset module, showing the configurable parameters for conversion of input files, creation of MISARA data structures, and to retrieve waveforms and channel metadata. The color version of this figure is available only in the electronic edition.

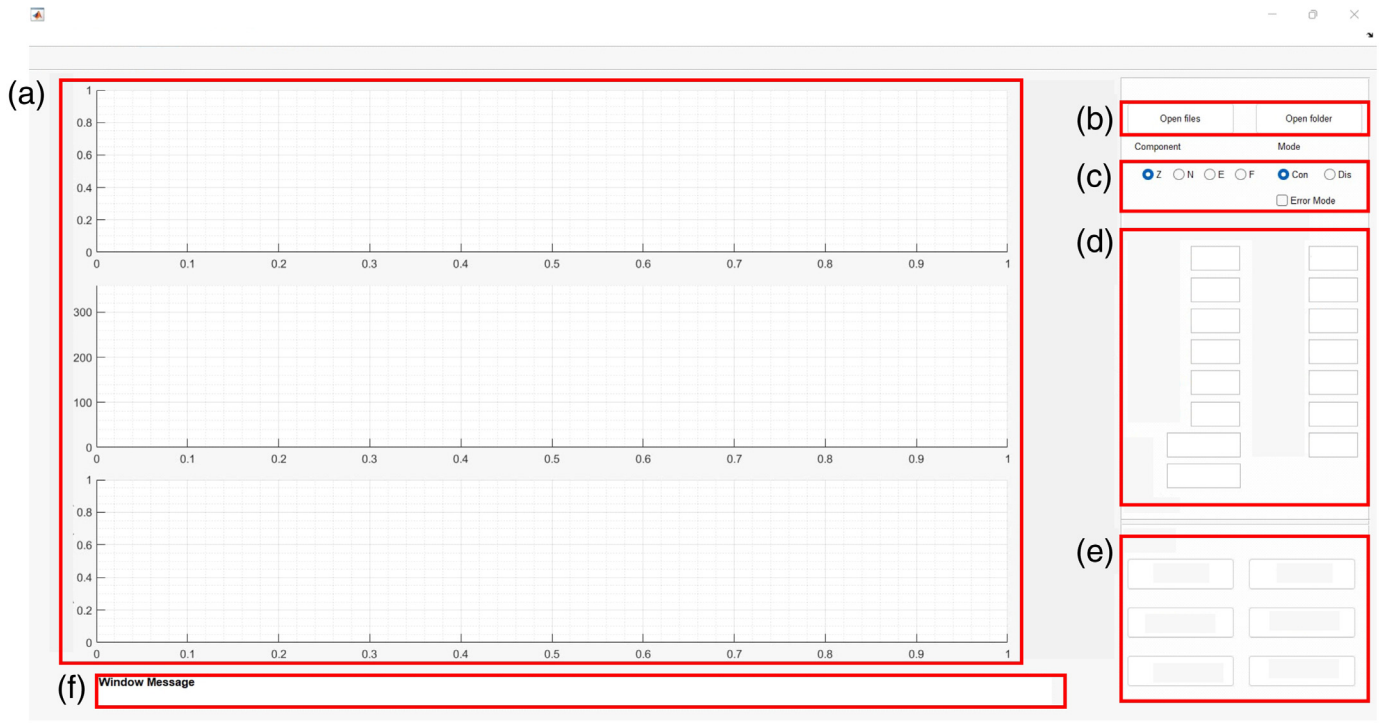

Figure 4. Example of the generic structure of MISARA modules. (a) Results plot panel; (b) data import panel; (c) panel for additional data selection or management of additional functionalities (e.g., channel selection or error calculations); (d) panel for setup of temporary parameters that affects the current analyses and its output; (e) control panel for processes within the module, such as visualization of results, data, and figure outputs; and (f) text window, displaying any information about data processing including errors, warnings, or command prompt messages. The color version of this figure is available only in the electronic edition.

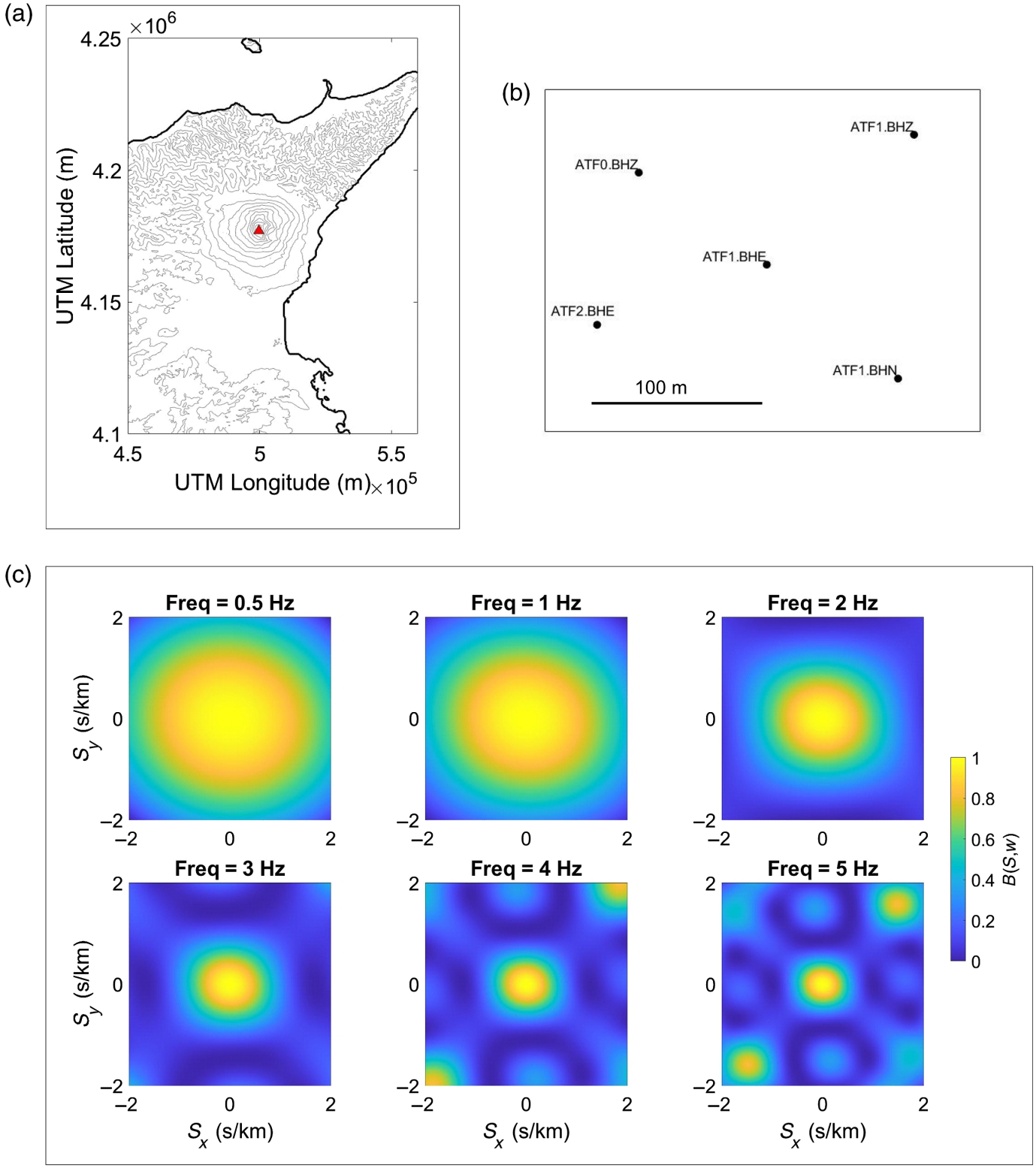

Figure 5. Output from the beam pattern module for a seismic array deployed at Mt. Etna during 2011. (a) Array location (red triangle) at Mt. Etna, East Sicily, Italy. (b) Detail of array geometry showing five sensors and an array aperture of ~200 m. All sensors are single-component Lennartz LE-3D/20 s seismometers. (c) Array response functions plotted at 0.5, 1.0, 2.0, 3.0, 4.0, and 5.0 Hz. The color version of this figure is available only in the electronic edition.

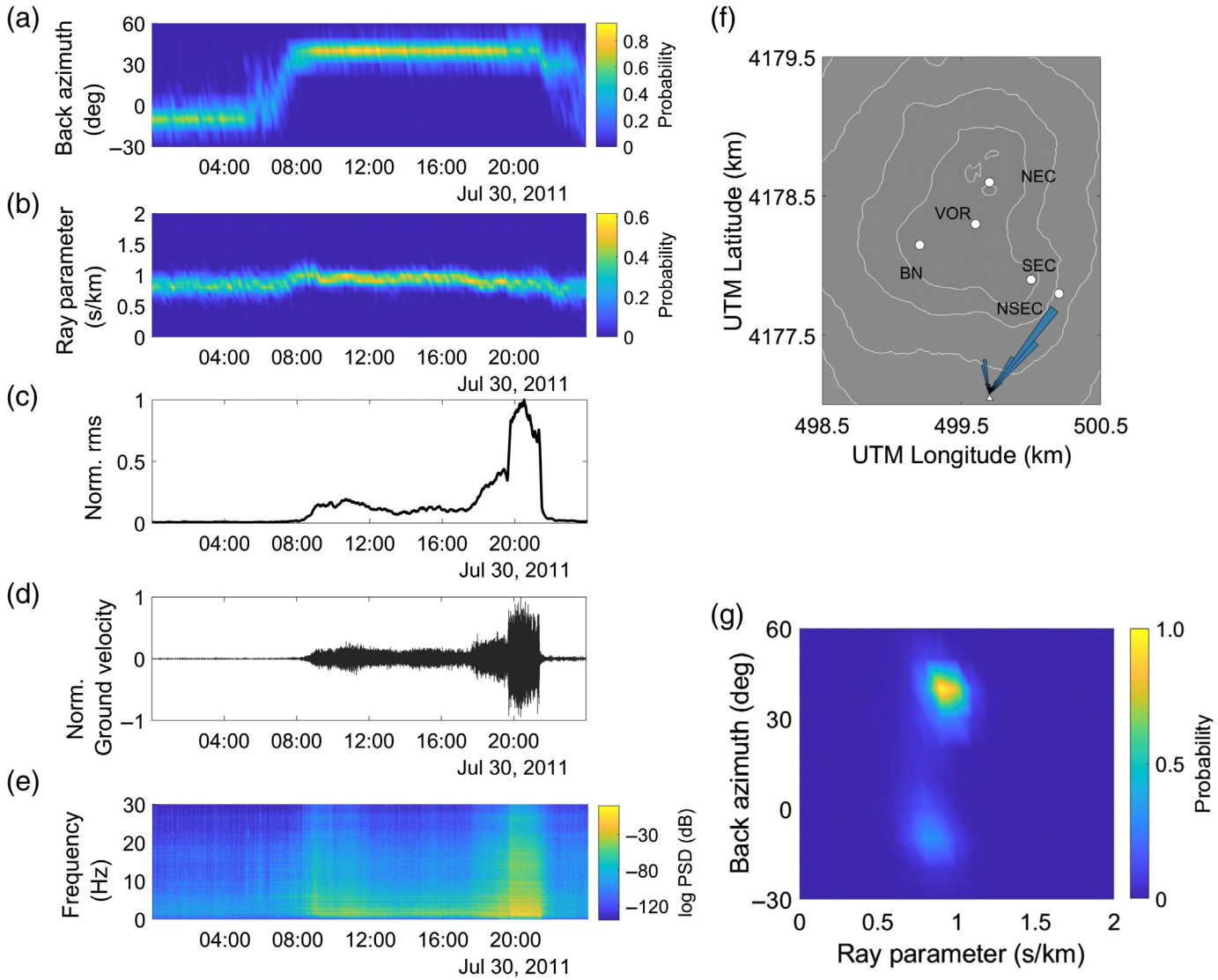

Nazionale di Geofisica e Vulcanologia (INGV). We used signals recorded by seven stations deployed in the summit area of Mt. Etna. These stations consisted of three-component, Trillium 40 s, seismometers (NanometricsTM) recording at a sampling rate of 100 Hz. An overview of the configuration and software performance for this case study is shown in Table A2. Using the STA/LTA and SALPED modules, we automatically detected LP and VLP events on 23 October 2010 (Fig. 7), when the BN crater produced moderate-to-intense Strombolian activity. We selected events based on their features, such as frequency content (Fig. 7a), characteristic waveform (Fig. 7b), and particle motion of the signals (Fig. 7c).

Under the assumption of a homogeneous and isotropic propagation medium (wave velocity of 1.6 km/s), and thus of spherical wavefronts, we used the semblance and radial semblance methods to track the source location of LP and VLP events, respectively. These two methods, based on waveform stacking, are similar to backprojection (Haney, 2014). Unlike backprojection, the semblance method achieves the

Figure 6. Output from the signal viewer, spectrogram, and zero lag cross-correlation (ZLC) analysis modules from analyses of volcanic tremor recorded on 30 July 2011 at Mt. Etna, Italy. (a) Temporal evolution of the array-calculated back azimuth. The back azimuth ranges between −15° and 5° N, during quiescent periods, and between 30° and 50° N during eruptive activity. (b) Temporal evolution of the seismic ray parameter. The parameter is observed to increase at the onset of eruptive activity from 0.6–1.0 to 0.7–1.2 s/km, possibly indicating a source migrating at shallower depth. The ZLC analysis performed on data were filtered in the 1.0–1.5 Hz frequency band; (a,b) back azimuths calculated for data windows with array cross-correlation coefficients greater than 0.75; (c) 1 hr long moving average of root mean square (rms) amplitudes in the 1.0–1.5 Hz frequency range at the central node of the array. (d) Seismic signal at the central node of the array. (e) Spectrogram at the central node of the array. (f) Polar histogram of back-azimuth results in (a) and plotted on the digital elevation model of the summit area of Mt. Etna with the main craters (white circles; BN, Bocca Nuova; VOR, Voragine; NEC, Northeast crater; SEC, Southeast crater; NSEC, New Southeast crater). (g) Bivariate distribution (2D histogram) of ray parameter and back azimuth shown in panels (a) and (b), respectively. The color version of this figure is available only in the electronic edition.

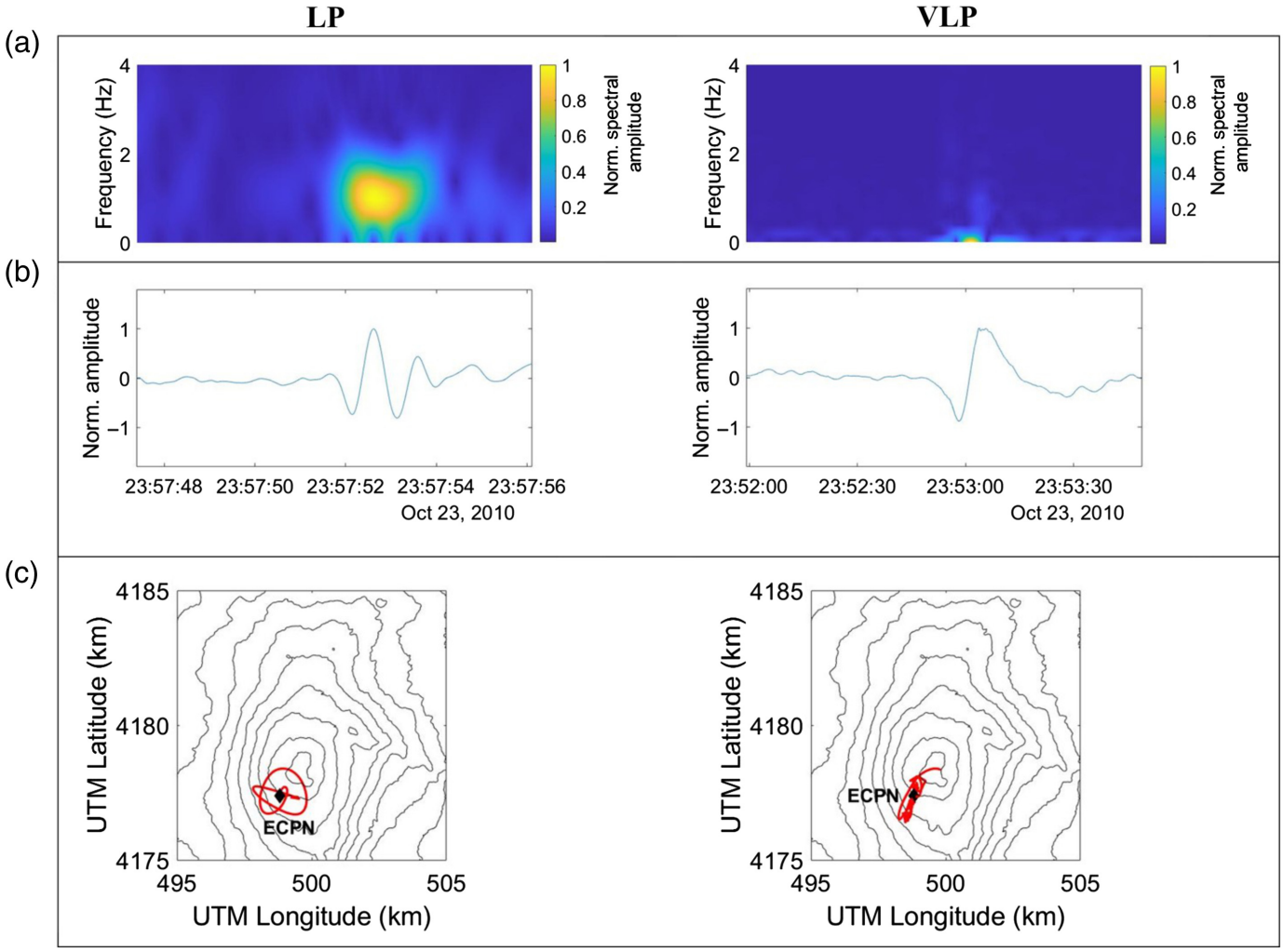

Figure 7. Examples of output from the sub-band automatic LP 39 events detection (SALPED) and short-term average/long-term average (STA/LTA) modules for detection and particle motion analyses of long-period (LP) and very long period (VLP) events recorded on 23 October 2010 at ECPN station. (a) Spectrograms of an example LP and VLP events and (b) their waveform in displacement, (c) particle motion of the LP and VLP signals. The color version of this figure is available only in the electronic edition.

best performances on the radial components of the wavefield, whereas radial semblance cannot be applied to nonradial components of the wavefield (Almendros *et al.*, 2002). We employed a grid-search approach using the signals recorded by seven INGV stations deployed in the summit area of Mt. Etna (Fig. 8). The results of our analyses are shown in Figure 8. The LP (Fig. 8a) and VLP (Fig. 8b) events were located below the BN crater at shallow depths—a common occurrence at Mt. Etna (e.g., Saccorotti *et al.*, 2007; Cannata *et al.*, 2009; Patanè *et al.*, 2013; Zuccarello *et al.*, 2013).

Case study 3: Mt. Etna, 2019 infrasound array

MISARA was also tested using data from a small-aperture infrasound array deployed at Mt. Etna in 2019. The data used here were already analyzed in De Angelis *et al.* (2020). The reader is refereed to this publication for additional information on this dataset. In particular, we focused on the infrasound waveforms recorded on 19 July 2019, when the NSEC produced intense explosive activity. We configured MISARA to mimic the analysis in De Angelis *et al.* (2020). A brief summary on the parameters configuration and performances of MISARA for this case study is shown in Table A3.

An example of analysis of these data with MISARA is shown in Figure 9. We used the spectrogram and ZLC modules to evaluate the main features and source position of the infrasound signal. The results of the analysis in Figure 9 are in agreement with De Angelis *et al.* (2020). In particular, Figure 9a shows back azimuths focused on 60° N, pointing toward the NSEC (Fig. 9e), as well as an increase in infrasound amplitude during the intensification of explosive activity (Fig. 9b–d).

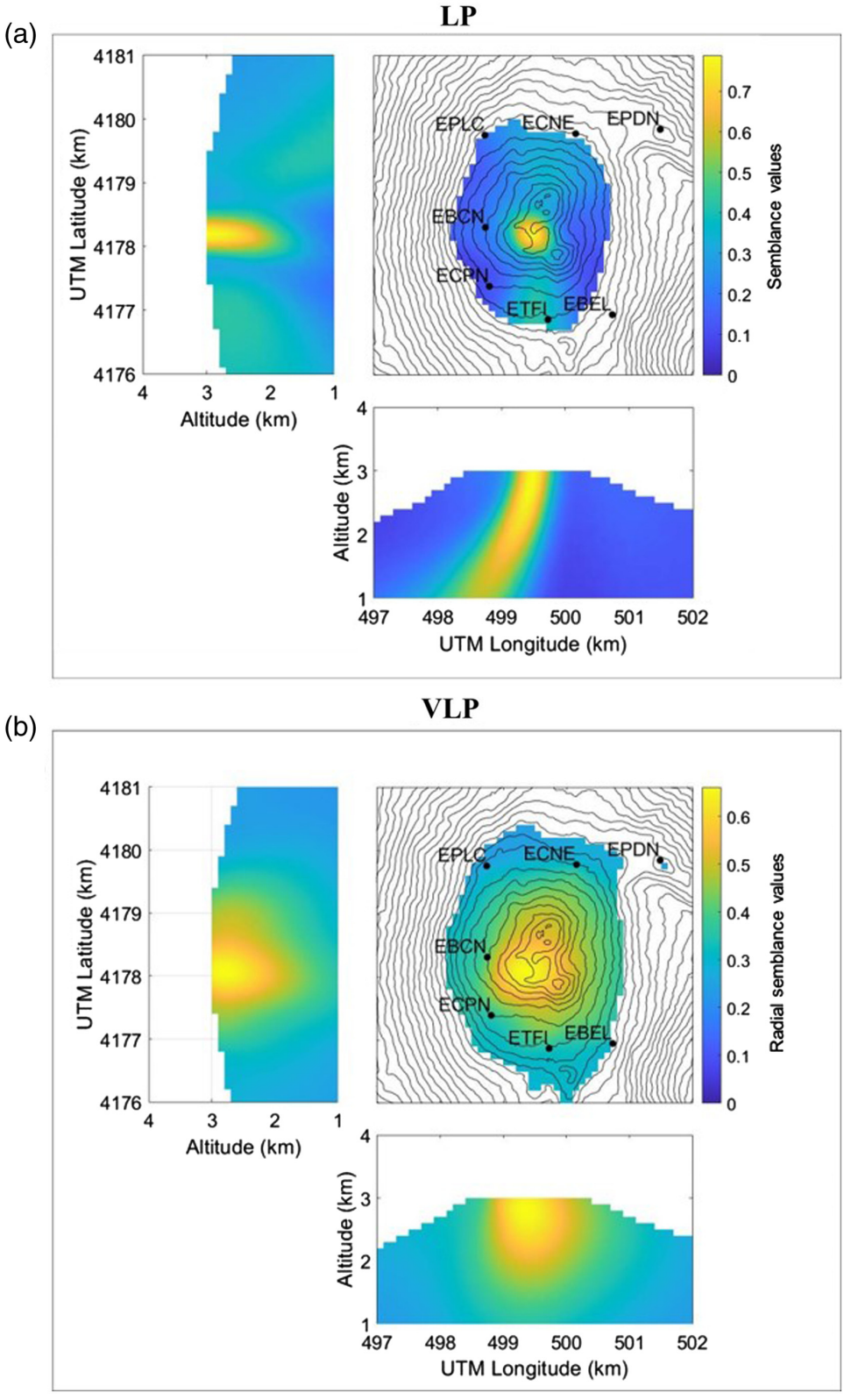

Figure 8. Examples of outputs of the semblance and radial semblance modules for the analyses of LP and VLP events recorded on 23 October 2010. Three sections of (a) semblance and (b) radial semblance grids through the largest value node; the results shown are average distributions for (a) 38 LPs and (b) 51 VLP, respectively; the grid of 5 × 5 × 2 km^3 (east–west, north–south, and vertical directions) is interpolated to the digital elevation model of Mt. Etna. The color version of this figure is available only in the electronic edition.

Conclusions

We have presented MISARA, an open-source MATLAB-based GUI designed to perform analyses of seismic and acoustic waveform data. A suite of well-established algorithms for volcano seismic and acoustic signal processing have been integrated into the GUI, with a focus on array techniques. Although MISARA was developed to facilitate the analysis of seismic and acoustic signals in volcanic environments, it can be used for other research purposes.

The modular structure of MISARA (Fig. 1) offers the flexibility to easily integrate additional functionalities. Most data processing tasks in MISARA are automated, reducing user's errors, and efforts. All processing parameters can be modified directly from within each module (Fig. 4), easily allowing multiple analyses on the same dataset. The modular structure offers input–output flexibility (Fig. 4).

Efficient algorithms with low computational cost are key for real-time or quasi-real-time analyses of large amounts of data. Although MISARA does not currently support real-time data processing, its algorithm implementation meets the requirements for monitoring applications (e.g., Chao *et al.*, 2017; Smith and Bean, 2020). Using a laptop with intermediate-to-high specifications (8 cores, 2.90 GHz Intel(R) Core (TM) i7-10700 CPU, 16 GB RAM), the processing times for the test cases (Tables A1, A2; Fig. A1) are of the order of few seconds to minutes for 1 day of data.

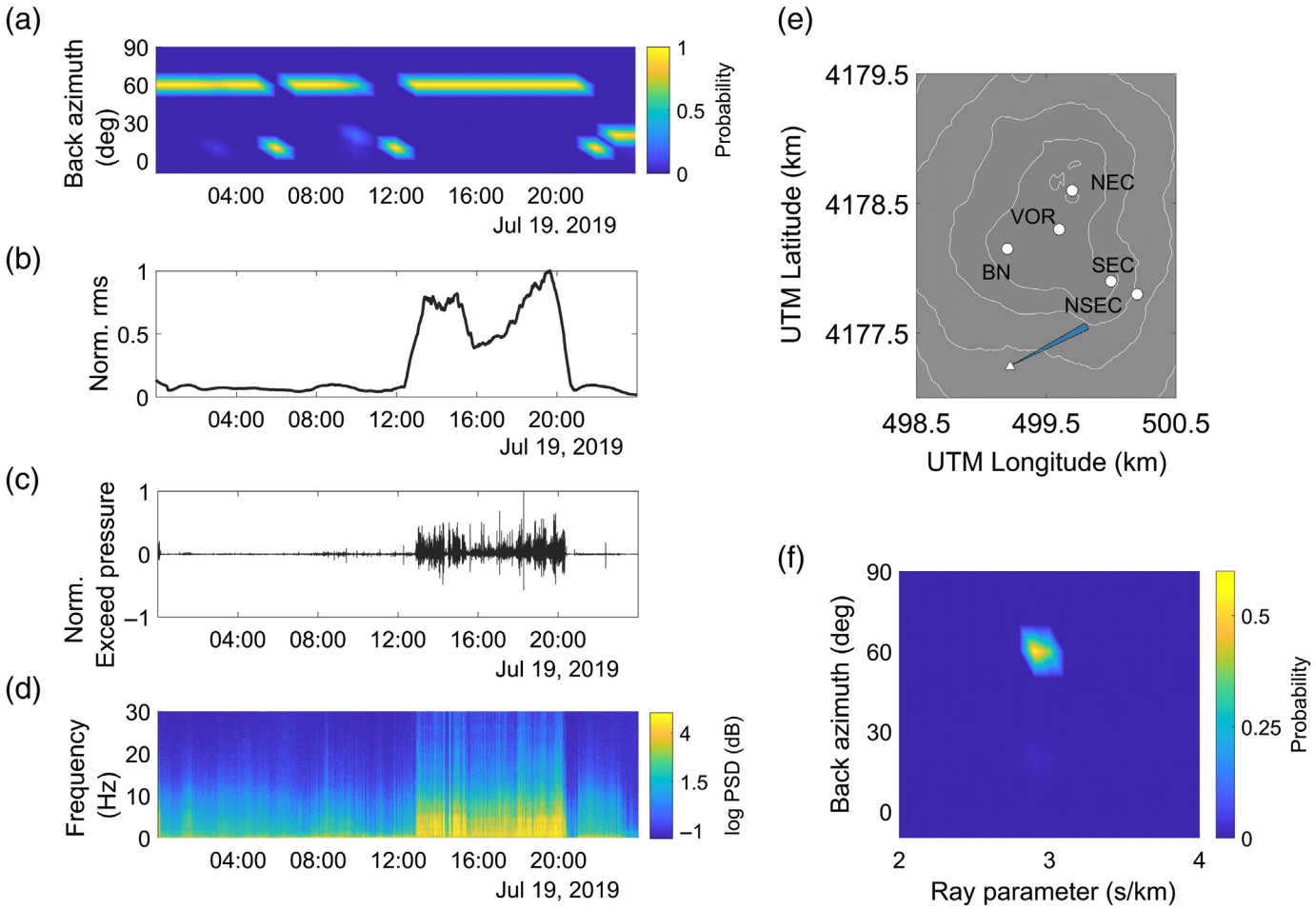

Figure 9. Output from the signal viewer, spectrogram, and ZLC modules from analyses of infrasonic tremor recorded on 30 July 2011 at Mt. Etna, Italy. (a) Temporal evolution of the array calculated back azimuth, ranging between 50° and 65° N. The ZLC analysis was performed on data were filtered in the 0.7–15 Hz frequency band. (b) The 1 hr long moving average of rms amplitudes in the 0.7–15 Hz frequency range at the central node of the array. (c) Infrasound signal at the central node of the array. (d) Spectrogram at the central node of the array. (e) Polar histogram of back-azimuth results in (a) and plotted on the digital elevation model of the summit area of Mt. Etna with the main craters (white circles). (f) Bivariate distribution (2D histogram) of ray parameter and back azimuth, respectively. The color version of this figure is available only in the electronic edition.

The software is suitable for applications including academic research, teaching, and analysis of data from temporary deployments. Future developments will support the use of MISARA for operational purposes. Although MISARA offers a user-friendly interface for the analysis of seismic and acoustic data from network and arrays, we acknowledge some possible limitations. For example, data preformatting routines in MISARA provide an alternative to the Python-based input and preprocessing procedures described in ObsPy (Beyreuther *et al.*, 2010). In its current configuration, MISARA allows uploading data in a fast and clear manner, avoiding the repetition of any preprocessing routine in different modules of the software or overloading the working memory. However, these routines could lead to duplication of data to the detriment of the storage requirements.

Future work to improve the capabilities of MISARA will be aimed at: (1) further simplifying the design and the structure of the software, providing an even more user-friendly GUI, (2) fully automate every stage of data input and processing, (3) implementing additional methods for more a more comprehensive investigation of seismic and acoustic data (e.g., De Barros *et al.*, 2011; Zuccarello *et al.*, 2016; Montesinos *et al.*, 2021), (4) adapting the GUI for real-time data processing and the exploitation of data streams provided by web services (e.g., Smith and Bean, 2020), and (5) integrating the GUI with well-established python libraries, such as ObsPy (Beyreuther *et al.*, 2010).

Data and Resources

The Matlab Interface for Seismo-Acoustic aRray Analysis (MISARA), its user's manual, and test data can be available at doi: 10.5281/zenodo.7410076. The seismic and infrasound data used in this article were obtained from Istituto Nazionale di Geofisica e Vulcanologia (INGV), Osservatorio Etneo-Sezione di Catania (https://www.ct.ingv.it/). The

commercial platform, MATLAB, is from Mathworks, available at http://www.mathworks.com. A MATLAB script to download the Incorporated Research Institutions for Seismology (IRIS) seismic data archive can be found at https://ds.iris.edu/ds/nodes/dmc/manuals/irisfetchm/. For the management of the DSS-Cube/Data-Cube3 files, gipptools package is available at https://www.gfz-potsdam.de/en/section/geophysical-imaging/infrastructure/geophysical-instrument-pool-potsdam-gipp/software/gipptools/. Additional details on Seismic Analysis Code (SAC) and Standard for the Exchange of Earthquake Data (SEED) formats are available at http://www.iris.edu/manuals/. All websites were last accessed in February 2023.

Declaration of Competing Interests

The authors acknowledge that there are no conflicts of interest recorded.

Acknowledgments

L. Zuccarello is supported by the project SINFONIA, progetto Bando Ricerca Libera 2021 Delibera 214/2021-INGV, by the Istituto Nazionale di Geofisica e Vulcanologia (INGV) Pianeta Dinamico 2021 Tema 8 SOME project (Grant Number CUP D53J1900017001) and by the INGV Pianeta Dinamico 2023-2025 VT_DYNAMO (Grant Number CUP D53J1900017001) project funded by the Italian Ministry of University and Research "Fondo finalizzato al rilancio degli investimenti delle amministrazioni centrali dello Stato e allo sviluppo del Paese, legge 145/2018." S. De Angelis is supported by NERC Grant Number NE/W004771/1. The authors thank the seismological technical staff of the INGV, Osservatorio Etneo-Sezione di Catania, for their support in the acquisition of seismic data.

References

Aki, K., and P. G. Richards (1980). *Quantitative Seismology*, W.H. Freeman, San Francisco, California, doi: 10.1002/gj.3350160110.

Allen, R. V. (1978). Automatic earthquake recognition and timing from single traces, *Bull. Seismol. Soc. Am.* **68,** no. 5, 1521–1532, doi: 10.1785/BSSA0680051521.

Almendros, J., B. Chouet, P. Dawson, and T. Bond (2002). Identifying elements of the plumbing system beneath Kilauea Volcano, Hawaii, from the source locations of very-long-period signals, *Geophys. J. Int.* **148,** no. 2, 303–312, doi: 10.1046/j.1365-246X.2002.01629.x.

Beyreuther, M., R. Barsch, L. Krischer, T. Megies, Y. Behr, and J. Wassermann (2010). ObsPy: A Python toolbox for seismology, *Seismol. Res. Lett.* **81,** no. 3, 530–533, doi: 10.1785/gssrl.81.3.530.

Bueno, A., L. Zuccarello, A. D. Moreno, J. Woollam, M. Titos, C. Benítez, I. Álvarez, J. Prudencio, and S. De Angelis (2020). PICOSS: Python interface for the classification of seismic signals, *Comput. Geosci.* **142,** doi: 10.1016/j.cageo.2020.104531.

Cannata, A., G. Di Grazia, M. Aliotta, C. Cassisi, P. Montalto, and D. Patanè (2013). Monitoring seismo-volcanic and infrasonic signals at volcanoes: Mt. Etna case study, *Pure Appl. Geophys.* **170,** no. 11, 1751–1771, doi: 10.1007/s00024-012-0634x.

Cannata, A., G. Di Grazia, P. Montalto, F. Ferrari, G. Nunnari, D. Patanè, and E. Privitera (2010). New insights into banded tremor from the 2008–2009 Mount Etna eruption, *J. Geophys. Res.* **115,** no. B12, doi: 10.1029/2009JB007120.

Cannata, A., M. Hellweg, G. Di Grazia, S. Ford, S. Alparone, S. Gresta, P. Montalto, and D. Patanè (2009). Long period and very long period events at Mt. Etna volcano: Characteristics, variability and causality, and implications for their sources, *J. Volcanol. Geotherm. Res.* **187,** nos. 3/4, 227–249, doi: 10.1016/j.jvolgeores.2009.09.007.

Capon, J. (1969). High-resolution frequency-wavenumber spectrum analysis, *Proc. IEEE* **57,** no. 8, 1408–1418, doi: 10.1109/PROC.1969.7278.

Carbone, D., L. Zuccarello, and G. Saccorotti (2008). Geophysical indications of magma uprising at Mt Etna during the December 2005 to January 2006 non-eruptive period, *Geophys. Res. Lett.* **35,** no. 6, doi: 10.1029/2008GL033212.

Chao, W. A., Y. M. Wu, L. Zhao, H. Chen, Y. G. Chen, J. M. Chang, and C. M. Lin (2017). A first near real-time seismology-based landquake monitoring system, *Sci. Rep.* **7,** no. 1, 1–12, doi: 10.1038/srep43510.

Chouet, B. A., and R. S. Matoza (2013). A multi-decadal view of seismic methods for detecting precursors of magma movement and eruption, *J. Volcanol. Geotherm. Res.* **252,** 108–175, doi: 10.1016/j.jvolgeores.2012.11.013.

Coombs, M. L., A. G. Wech, M. M. Haney, J. J. Lyons, D. J. Schneider, H. F. Schwaiger, K. L. Wallace, D. Fee, J. T. Freymueller, J. R. Schaefer, *et al.* (2018). Short-term forecasting and detection of explosions during the 2016–2017 eruption of Bogoslof volcano, Alaska, *Front. Earth Sci.* **6,** 122, doi: 10.3389/feart.2018.00122.

Cortés, G., R. Carniel, P. Lesage, M. Á. Mendoza, and I. Della Lucia (2021). Practical volcano-independent recognition of seismic events: VULCAN.ears project, *Front. Earth Sci.* **8,** 616676, doi: 10.3389/feart.2020.616676.

De Angelis, S., M. M. Haney, J. J. Lyons, A. Wech, D. Fee, A. Diaz-Moreno, and L. Zuccarello (2020). Uncertainty in detection of volcanic activity using infrasound arrays: Examples from Mt. Etna, Italy, *Front. Earth Sci.* **8,** 169, doi: 10.3389/feart.2020.00169.

De Angelis, S., L. Zuccarello, S. Rapisarda, and V. Minio (2021). Introduction to a community dataset from an infrasound array experiment at Mt. Etna, Italy, *Sci. Data* **8,** no. 1, 1–9, doi: 10.1038/s41597-021-01030-6.

De Barros, L., I. Lokmer, C. J. Bean, G. S. O'Brien, G. Saccorotti, J. P. Métaxian, L. Zuccarello, and D. Patanè (2011). Source mechanism of long-period events recorded by a high-density seismic network during the 2008 eruption on Mount Etna, *J. Geophys. Res.* **116,** no. B1, doi: 10.1029/2010JB007629.

Di Grazia, G., S. Falsaperla, and H. Langer (2006). Volcanic tremor location during the 2004 Mount Etna lava effusion, *Geophys. Res. Lett.* **33,** no. 4, doi: 10.1029/2005GL025177.

Di Lieto, B., G. Saccorotti, L. Zuccarello, M. L. Rocca, and R. Scarpa (2007). Continuous tracking of volcanic tremor at Mount Etna, Italy, *Geophys. J. Int.* **169,** no. 2, 699–705, doi: 10.1111/j.1365-246X.2007.03316.x.

Efron, B. (1982). *The Jackknife, the Bootstrap and Other Resampling Plans*, Society for Industrial and Applied Mathematics, Philadelphia, Pennsylvania, doi: 10.1137/1.9781611970319.

Eibl, E. P., C. J. Bean, K. S. Vogfjörd, Y. Ying, I. Lokmer, M. Möllhoff, G. S. O'Brien, and F. Pálsson (2017). Tremor-rich shallow dyke formation followed by silent magma flow at Bárðarbunga in Iceland, *Nature Geosci.* **10,** no. 4, 299–304, doi: 10.1038/ngeo2906.

Euler, G. (2014). Project SEIZMO, available at: http://epsc.wustl.edu/ggeuler/codes/m/seizmo/ (last accessed February 2023).

Frankel, A., S. Hough, P. Friberg, and R. Busby (1991). Observations of Loma Prieta aftershocks from a dense array in Sunnyvale, California, *Bull. Seismol. Soc. Am.* **81,** no. 5, 1900–1922, doi: 10.1785/BSSA0810051900.

Garcia, L., I. Alvarez, M. Titos, A. D. Moreno, M. C. Benıtez, and A. de la Torre (2017). Automatic detection of long period events based on subband-envelope processing, *IEEE J. Sel. Top. Appl. Earth Obs. Remote Sens.* **10,** no. 11, 5134–5142, doi: 10.1109/jstars.2017.2739690.

Goldstein, P., and A. Snoke (2005). SAC availability for the IRIS Community, *Incorporated Research Institutions for Seismology Newsletter*, 7(UCRL-JRNL-211140), available at https://www.osti.gov/servlets/purl/875360i (last accessed February 2023).

Goldstein, P., D. Dodge, M. Firpo, L. Minner, W. Lee, H. Kanamori, P. Jennings, and C. Kisslinger (2003). SAC2000: Signal processing and analysis tools for seismologists and engineers, invited contribution to *The IASPEI International Handbook of Earthquake and Engineering Seismology*,W. H. K. Lee, H. Kanamori, P. C. Jennings, and C. Kisslinger (Editors) Academic Press, London, United Kingdom.

Haney, M. M. (2014). Backprojection of volcanic tremor, *Geophys. Res. Lett.* **41,** 1923–1928, doi: 10.1002/2013GL058836.

Haney, M. M., J. Power, M. West, and P. Michaels (2012). Causal instrument corrections for short-period and broadband seismometers, *Seismol. Res. Lett.* **83,** no. 5, 834–845, doi: 10.1785/0220120031.

Havskov, J., and G. Alguacil (2016). Seismic arrays, in *Instrumentation in Earthquake Seismology*, Springer, Cham, Switzerland, 309–329, doi: 10.1007/978-3-319-21314-9_9.

Inza, L. A., J. P. Métaxian, J. I. Mars, C. J. Bean, G. S. O'Brien, O. Macedo, and D. Zandomeneghi (2014). Analysis of dynamics of vulcanian activity of Ubinas volcano, using multicomponent seismic antennas, *J. Volcanol. Geotherm. Res.* **270,** 35–52, doi: 10.1016/j.jvolgeores.2013.11.008.

Jurkevics, A. (1988). Polarization analysis of three-component array data, *Bull. Seismol. Soc. Am.* **78,** no. 5, 1725–1743, doi: 10.1785/BSSA0780051725.

Kenney, J. F., and E. S. Keeping (1962). Root mean square, in *Mathematics of Statistics, Pt. 1*, Third Ed., D. Van Nostrand Company, Princeton, New Jersey, 59–60.

Lesage, P. (2009). Interactive Matlab software for the analysis of seismic volcanic signals, *Comput. Geosci.* **35,** no. 10, 2137–2144, doi: 10.1016/j.cageo.2009.01.010.

Löer, K., N. Riahi, and E. H. Saenger (2018). Three-component ambient noise beamforming in the Parkfield area, *Geophys. J. Int.* **213,** no. 3, 1478–1491, doi: 10.1093/gji/ggy058.

McNutt, S. R., G. Thompson, J. Johnson, S. De Angelis, and D. Fee (2015). Seismic and infrasonic monitoring, in *The Encyclopedia of Volcanoes*, H. Sigurdsson (Editor), Academic Press, Amsterdam, Holland, 1071–1099, doi: 10.1016/B978-0-12-385938-9.00063-8.

Messina, A., and H. Langer (2011). Pattern recognition of volcanic tremor data on Mt. Etna (Italy) with KKAnalysis—A software program for unsupervised classification, *Comput. Geosci.* **37,** no. 7, 953–961, doi: 10.1016/j.cageo.2011.03.015.

Montesinos, B. M., C. J. Bean, and I. Lokmer (2021). Quantifying strong seismic propagation effects in the upper volcanic edifice using sensitivity kernels, *Earth Planet. Sci. Lett.* **554,** doi: 10.1016/j.epsl.2020.116683.

Morioka, H., H. Kumagai, and T. Maeda (2017). Theoretical basis of the amplitude source location method for volcano-seismic signals, *J. Geophys. Res.* **122,** no. 8, 6538–6551, doi: 10.1002/2017JB013997.

Moschella, S., A. Cannata, G. Di Grazia, and S. Gresta (2018). Insights into lava fountain eruptions at Mt. Etna by improved source location of the volcanic tremor, *Ann. Geophys.* doi: 10.4401/ag-7552.

Patanè, D., A. Aiuppa, M. Aloisi, B. Behncke, A. Cannata, M. Coltelli, G. Di Grazia, S. Gambino, S. Gurrieri, M. Mattia, *et al.* (2013). Insights into magma and fluid transfer at Mount Etna by a multiparametric approach: A model of the events leading to the 2011 eruptive cycle, *J. Geophys. Res.* **118,** no. 7, 3519–3539, doi: 10.1002/jgrb.50248.

Pignatelli, A., A. Giuntini, and R. Console (2008). Matlab software for the analysis of seismic waves recorded by three-element arrays, *Comput. Geosci.* **34,** no. 7, 792–801, doi: 10.1016/j.cageo.2007.10.003.

Rost, S., and C. Thomas (2002). Array seismology: Methods and applications, *Rev. Geophys.* **40,** no. 3, 1008, doi: 10.1029/2000RG000100.

Saccorotti, G., I. Lokmer, C. J. Bean, G. Di Grazia, and D. Patanè (2007). Analysis of sustained long-period activity at Etna Volcano, Italy, *J. Volcanol. Geotherm. Res.* **160,** nos. 3/4, 340–354, doi: 10.1016/j.jvolgeores.2006.10.008.

Saccorotti, G., L. Zuccarello, E. Del Pezzo, J. Ibáñez, and S. Gresta (2004). Quantitative analysis of the tremor wavefield at Etna Volcano, Italy, *J. Volcanol. Geotherm. Res.* **136,** 223–245, doi: 10.1016/j.jvolgeores.2004.04.003.

Schlindwein, V., J. Wassermann, and F. Scherbaum (1995). Spectral analysis of harmonic tremor signals at Mt. Semeru volcano, Indonesia, *Geophys. Res. Lett.* **22,** no. 13, 1685–1688, doi: 10.1029/95GL01433.

Schmidt, R. O. (1986). Multiple emitter location and signal parameter estimation, *IEEE Trans. Antennas Propag.* **34,** 276–280, doi: 10.1109/TAP.1986.1143830.

Smith, P. J., and C. J. Bean (2020). RETREAT: A REal-Time TREmor analysis tool for seismic arrays, with applications for volcano monitoring, *Front. Earth Sci.* **8,** doi: 10.3389/feart.2020.586955.

Sparks, R. S. J., J. Biggs, and J. W. Neuberg (2012). Monitoring volcanoes, *Science* **335,** no. 6074, 1310–1311, doi: 10.1126/science.1219485.

Thompson, G., and C. Reyes (2018). GISMO-A seismic data analysis toolbox for MATLAB [software package], available at http://geoscience communitycodes.github.io/GISMO/ (last accessed February 2023).

Wathelet, M., B. Guillier, P. Roux, C. Cornou, and M. Ohrnberger (2018). Rayleigh wave three-component beamforming: Signed ellipticity assessment from high-resolution frequency-wavenumber processing of ambient vibration arrays, *Geophys. J. Int.* **215,** no. 1, 507–523, doi: 10.1093/gji/ggy286.

Welch, P. (1967). The use of fast Fourier transform for the estimation of power spectra: A method based on time averaging over short,

modified periodograms, *IEEE Trans. Audio Electroacoust.* **15,** no. 2, 70–73, doi: 10.1109/TAU.1967.1161901.

Zuccarello, L., M. R. Burton, G. Saccorotti, C. J. Bean, and D. Patanè (2013). The coupling between very long period seismic events, volcanic tremor, and degassing rates at Mount Etna volcano, *J. Geophys. Res.* **118,** no. 9, 4910–4921, doi: 10.1002/jgrb.50363.

Zuccarello, L., S. De Angelis, V. Minio, G. Saccorotti, C. J. Bean, M. Paratore, and J. Ibáñez (2022). Volcanic tremor tracks changes in multi-vent activity at MountEtna, Italy: Evidence from analyses of seismic array data, *Geophys. Res. Lett.* **49,** doi: 10.1029/2022GL100056.

Zuccarello, L., M. Paratore, M. La Rocca, F. Ferrari, A. Messina, S. Branca, D. Contrafatto, D. Galluzzo, and S. Rapisarda (2016). Shallow velocity model in the area of Pozzo Pitarrone, Mt. Etna, from single station, array methods and borehole data, *Ann. Geophys.* doi: 10.4401/ag-7086.

Appendix

In this appendix, the performance of MISARA was evaluated by computing the overall time required to apply each method or routine for the three cases of study. A comparison of these times is shown in Figure A1. More details about the performance of the software are resumed in Tables A1–A3. These tables also indicate the configuration of the parameters used to perform all analyses in the three cases of study.

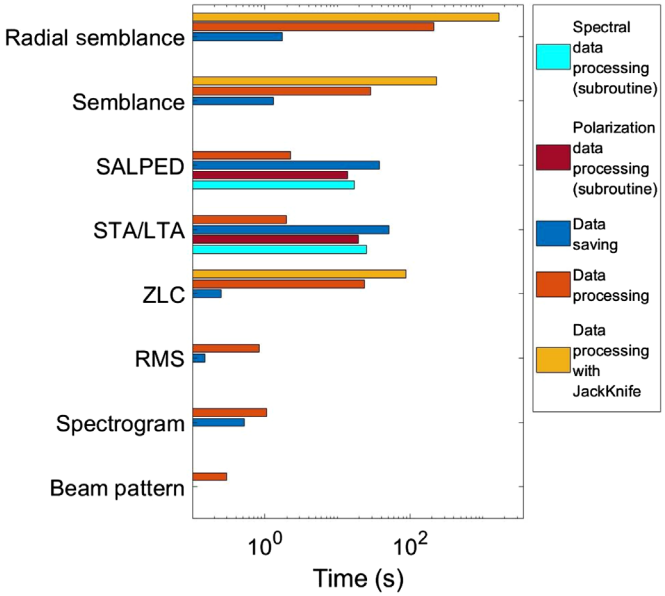

Figure A1. Software performance for Test Case study 1, 2, and 3. Each bar refers to the overall time required to perform the analyses summarized in Tables A1–A3. The legend to the right side of the diagram refers to the types of routines–subroutines activated during the processing of the data. The color version of this figure is available only in the electronic edition.

TABLE A1
Parameters for Analysis of Volcanic Tremor Recorded on 30 July 2011 Using Beam Pattern, Spectrogram, and Zero Lag Cross-Correlation (ZLC) Modules

Method	Settings	Waveform Data	Output Size	Timing
Beam pattern	Frequency (Hz): 0.5–5.0, frequency step (Hz): 0.5, grid size (s^2/km^2): 2 × 2, grid step (s/km): 0.05			Data processing (s): ∼0.30
Spectrogram	Window (s): 60, *N*° samples spectra: 8192, high-pass filter (Hz): 0.01, averaging factor (min): 30	Sample rate (Hz): 100, sample count: 8,460,000, *N*° sensors: one vertical component	∼2.41 MB	Data processing (s): ∼1.07, data saving (s): ∼0.52
Root mean square (rms)	Window (s): 10, frequency band (Hz): 1.0–1.5, averaging factor (min): 60	Sample rate (Hz): 100, sample count: 8,460,000, *N*° sensors: one vertical component	∼117 KB	Data processing (s): ∼0.83, data saving (s): ∼0.15
ZLC	Window (s): 10, frequency band (Hz): 1.0–1.5, velocity waves (km/s): 1.6 km, maximum delay time (s): 4, spline interpolation: true, histogram bin (min): 60, correlation threshold: 0.75	Sample rate (Hz): 100, sample count: 8,460,000, *N*° sensors: five vertical component	∼579 KB	Data processing (s): ∼23.83, data processing with jackkinfe (s): ∼88.09, data saving (s): ∼0.25

TABLE A2
Parameter for the Analysis of LP and VLP Events Recorded on 23 October 2010 Using STA/LTA, SALPED, Semblance, and Radial Semblance Modules

Method	Settings	Waveform Data	Output Size	Timing
STA/LTA	Frequency band (Hz): 0.01–0.15, STA window (s): 6, LTA window (s): 60, detection threshold: 2.5, window spectrogram (s): 5.28, overlap window spectrogram (s): 5.20, N° samples spectra: 1,024, window polarization (s): 5	Sample rate (Hz): 100, sample count: 8,460,000, *N*° sensors: one three components	∼86.50 MB	Data processing (s): ∼1.97, spectral data processing (s): ∼24.99 (∼0.49 per event), polarization data processing (s): ∼19.38 (∼0.38 per event), data saving (s): ∼51.29 (∼1.01 per event)
SALPED	Central frequency brand (Hz): 0.5–1.2, lower frequency band (Hz): 0.1–0.4, upper frequency band (Hz): 3–10, windows (s): ±5, detection threshold: 1.0, window spectrogram (s): 1.28, overlap window spectrogram (s): 1.20, *N*° samples spectra: 128, window polarization (s): 2.5	Sample rate (Hz): 100, sample count: 8,460,000, *N*° sensors: one three components	∼11.70 MB	Data processing (s): ∼2.24, spectral data processing (s): ∼17.10 (∼0.45 per event), polarization data processing (s): ∼13.68 (∼0.36 per event), data saving (s): ∼38.22 (∼1.01 per event)
Semblance	Window (s): 2.5, frequency band (Hz): 0.5–1.2, central frequency (Hz): 1, grid size (km^3): 5 × 5 × 2, grid step (km): 0.1, quality factor: 40, velocity waves (km/s): 1.6 km, attenuation factor: 1	Sample rate (Hz): 100, sample count: 1,000, *N*° sensors: seven three components, *N*° events: 38	∼12.10 MB	Data processing (s): ∼28.72 (∼0.75 per event), data processing with jackkinfe (s): ∼230 (∼6.05 per event), data saving (s): ∼1.30
Radial semblance	Window (s): 5, frequency band (Hz): 0.01–0.15, grid size (km^3): 5 × 5 × 2, grid step (km): 0.1, velocity waves (km/s): 1.6 km	Sample rate (Hz): 100, sample count: 12,000, *N*° sensors: seven three components, *N*° events: 51	∼15. 30 MB	Data processing (s): ∼211.76 (∼4.15 per event), data processing with jackkinfe (s): ∼1 694.08 (∼33.22 per event), data saving (s): ∼1.75

LP, long period; STA/LTA, short-term average/long-term average; SALPED, Sub-band Automatic LP Events Detection; and VLP, very long period.

TABLE A3
Parameters for the Analysis of Infrasound Recorded on 19 July 2019 Using Spectrogram and ZLC Modules

Method	Settings	Waveform Data	Output Size	Timing
Spectrogram	Window (s): 60, *N*° samples spectra: 8,192, high-pass filter (Hz): 0.01, averaging factor (min): 30	Sample rate (Hz): 100, sample count: 8,460,000, *N*° sensors: one vertical component	∼1.86 MB	Data processing (s): ∼0.98, data saving (s): ∼0.37
Rms	Window (s): 10, frequency band (Hz): 0.7–15, averaging factor (min): 60	Sample rate (Hz): 100, sample count: 8,460,000, *N*° sensors: one vertical component	∼192 KB	Data processing (s): ∼0.81, data saving (s): ∼0.35
ZLC	Window (s): 10, frequency band (Hz): 0.7–15, velocity waves (km/s): 0.354 km, maximum delay time (s): 4, spline interpolation: true, histogram bin (min): 60, correlation threshold: 0.75	Sample rate (Hz): 100, sample count: 8,460,000, *N*° sensors: six vertical component	∼460 KB	Data processing (s): ∼24.01, data processing with jackkinfe (s): ∼87.54, data saving (s): ∼0.31

Manuscript received 23 August 2022
Published online 27 February 2023